Performance comparison of 0/π- and ± π/2-phase-shifted superstructured Fiber Bragg grating en/decoder

Bo Dai,[1] Zhensen Gao,[1] Xu Wang,[1,*] Nobuyuki Kataoka,[2] and Naoya Wada[2]

[1]*Joint Research Institute for Integrated Systems, Heriot-Watt University, Edinburgh, UK*
[2]*National Institute of Information and Communications Technology (NICT), Tokyo, Japan*
**x.wang@hw.ac.uk*

Abstract: We compare the performances of the 0/π-phase-shifted SSFBG (0/π-SSFBG) and the ± π/2-phase-shifted SSFBG (± π/2-SSFBG) en/decoders in the three aspects: the security, coding and system performances. In terms of the security performance, we evaluate the security performance by the investigation on the encoded waveform of both encoders. We also propose and demonstrate the code extraction technique for the ± π/2-SSFBG encoder when input pulse has large pulse width. Then, we analyze the coding performance of these two kinds of en/decoders by the calculation of autocorrelation and cross-correlation with sets of 31-chip, 63-chip and 127-chip Gold codes. Furthermore, we propose and demonstrate the hybrid use of both en/decoders. To demonstrate the performance of both en/decoders and the hybrid use in the different systems, we employ four 31-chip 640 Gchip/s 0/π-SSFBG and ± π/2-SSFBG en/decoders in the 4-user 10 Gbps/user on-off keying and differential phase-shift keying OCDMA systems.

OCIS codes: (060.3735) Fiber Bragg gratings; (060.4785) Optical security and encryption; (060.0060) Fiber optics and optical communications.

References and links

1. H. Tsuda, H. Takenouchi, T. Ishii, K. Okamoto, T. Goh, K. Sato, A. Hirano, T. Kurokawa, and C. Amano, "Spectral encoding and decoding of 10 Gbit/s femtosecond pulses using high resolution arrayed-waveguide grating," Electron. Lett. **35**(14), 1186–1188 (1999).
2. X. Wang, N. Wada, G. Cincotti, T. Miyazaki, and K. Kitayama, "Demonstration of over 128-gb/s-capacity (12-User/spl times/10.71-gb/s/user) asynchronous OCDMA using FEC and AWG-based multiport optical encoder/decoders," IEEE Photon. Technol. Lett. **18**(15), 1603–1605 (2006).
3. G. E. Town, K. Chan, and G. Yoffe, "Design and performance of high-speed optical pulse-code generators using optical fiber Bragg gratings," IEEE J. Sel. Top. Quantum Electron. **5**(5), 1325–1331 (1999).
4. P. C. Teh, P. Petropoulos, M. Ibsen, and D. J. Richardson, "A comparative study of the performance of seven- and 63-chip optical code-division multiple-access encoders and decoders based on superstructured fiber Bragg gratings," J. Lightwave Technol. **19**(9), 1352–1365 (2001).
5. A. Grunnet-Jepsen, A. E. Johnson, E. S. Maniloff, T. W. Mossberg, M. J. Munroe, and J. N. Sweetser, "Fiber Bragg grating based spectral encoder/decoder for lightwave CDMA," Electron. Lett. **35**(13), 1096–1097 (1999).
6. I. Fsaifes, A. Millaud, S. Cordette, C. Lepers, M. Douay, and C. Ware, "Spectral phase OCDMA encoder/decoder using travelling interference fringe photo-writing technique," Asia Commun. and Photon. (ACP' 09), **7630**, Shanghai, China (2009).
7. A. Agarwal, P. Toliver, R. Menendez, S. Etemad, J. Jackel, J. Young, T. Banwell, B. E. Little, S. T. Chu, Wei Chen, Wenlu Chen, J. Hryniewicz, F. Johnson, D. Gill, O. King, R. Davidson, K. Donovan, and P. J. Delfyett, "Fully programmable ring-resonator-based integrated photonic circuit for phase coherent applications," J. Lightwave Technol. **24**(1), 77–87 (2006).
8. X. Wang, K. Matsushima, A. Nishiki, N. Wada, and K. Kitayama, "High reflectivity superstructured FBG for coherent optical code generation and recognition," Opt. Express **12**(22), 5457–5468 (2004).
9. X. Wang, K. Matsushima, K. Kitayama, A. Nishiki, N. Wada, and F. Kubota, "High-performance optical code generation and recognition by use of a 511-chip, 640-Gchip/s phase-shifted superstructured fiber Bragg grating," Opt. Lett. **30**(4), 355–357 (2005).
10. Y. Dai, X. Chen, Y. Zhang, J. Sun, and S. Xie, "Phase-error-free, 1023-chip OCDMA en/de-coders based on reconstruction equivalent chirp technology and error-correction method," in Proc. Opt. Fiber Commun. Conf. (OFC' 06), paper JWA28, Anaheim, USA (2006).

#143119 - $15.00 USD Received 23 Feb 2011; revised 27 May 2011; accepted 1 Jun 2011; published 9 Jun 2011

11. Z. Si, F. Yin, M. Xin, H. Chen, M. Chen, and S. Xie, "Code extraction from encoded signal in time-spreading optical code division multiple access," Opt. Lett. **35**(2), 229–231 (2010).
12. B. Dai and X. Wang, "Security improvement using ±π/2-phase-shifted SSFBG en/decoder in time-spreading OCDMA," IEEE Photon. Technol. Lett. **22**(12), 881–883 (2010).
13. K. Sasaki, M. Sarashina, S. Kobayashi, H. Tamai, A. Nishiki, and T. Ushikubo, "A new π/2-shift-BPSK signal by superstructure fibre Bragg grating en/decoder," in Proc. European Conf. on Optical Commun. (ECOC' 05), paper We4.P.047, Glasgow, UK (2005).
14. P. C. Teh, M. Ibsen, J. H. Lee, P. Petropoulos, and D. J. Richardson, "Demonstration of a four-channel WDM/OCDMA system using 255-chip 320-Gchip/s quarternary phase coding gratings," IEEE Photon. Technol. Lett. **14**(2), 227–229 (2002).
15. X. Wang and K. Kitayama, "Analysis of beat noise in coherent and incoherent time-spreading OCDMA," J. Lightwave Technol. **22**(10), 2226–2235 (2004).
16. X. Wang, T. Hamanaka, N. Wada, and K. Kitayama, "Dispersion-flattened-fiber based optical thresholder for multiple-access-interference suppression in OCDMA system," Opt. Express **13**(14), 5499–5505 (2005).
17. N. Wada, H. Sotobayashi, and K. Kitayama, "Error-free 100km transmission at 10Gbit/s in optical code division multiplexing system using BPSK picosecond-pulse code sequence with novel time-gating detection," Electron. Lett. **35**(10), 833–834 (1999).
18. V. J. Hernandez, W. Cong, R. P. Scott, C. Yang, N. K. Fontaine, B. H. Kolner, J. P. Heritage, and S. J. B. Yoo, "320-Gb/s capacity (32 Users × 10 Gb/s) SPECTS O-CDMA local area network testbed," in Proc. Opt. Fiber Commun. Conf. (OFC' 06), paper PDP45, Anaheim, USA (2006).
19. P. Petropoulos, N. Wada, P. C. Teh, M. Ibsen, W. Chujo, K. Kitayama, and D. J. Richardson, "Demonstration of a 64-chip OCDMA system using superstructured fiber gratings and time-gating detection," IEEE Photon. Technol. Lett. **13**(11), 1239–1241 (2001).

1. Introduction

In the optical code division multiple access (OCDMA) system, optical coding (OC) devices are the crucial components for code generation and recognition. Many OC devices are proposed for the OCDMA system, such as arrayed waveguide grating (AWG) [1,2], fiber Bragg grating (FBG) [3–6] and microring resonator (MRR) [7]. Among these OC devices, FBG can be employed in both the coherent and incoherent OCDMA systems for the temporal or spectral phase coding with the advantages of low insertion loss, high compactness, polarization independent performance and low cost. In the coherent time-spreading OCDMA system, superstructured FBG (SSFBG) is applied for the phase coding, which is capable to generate ultra-long code with ultra-high chip rate [4,8–10].

Typically, 0/π-phase-shifted SSFBG (0/π-SSFBG) en/decoder, which has the structure of 0 or π phase shift between adjacent chips, is used for the temporal binary phase coding. However, the security vulnerability of the 0/π-SSFBG encoder has been revealed [11,12]. The cancellation of the adjacent chips, due to the π phase shift, resulting in a dip, implies the vulnerable regularity in the encoded waveform. Based on this regularity, in the single-user system, eavesdroppers can easily extract the code sequence from the encoded waveform. Using ± π/2-phase-shifted SSFBG (± π/2-SSFBG) en/decoder was proposed for the uniformity of the encoded waveform with different code patterns and to improve the security [12,13]. The ± π/2-SSFBG has the phase shift of either + π/2 or –π/2 between adjacent chips, subject to the code pattern. ± π/2-SSFBG encoder provides uniform encoded waveform, which is regardless of code pattern, significantly enhancing the security.

In this paper, we compare the security, coding and system performances of the 0/π-SSFBG and ± π/2-SSFBG en/decoders. In the Section II, we demonstrate the encoded waveforms of both 0/π-SSFBG and ± π/2-SSFBG encoders to evaluate the security performance. We also study the influence of the input pulse over the encoded waveform of the ± π/2-SSFBG encoder and summarize the code extraction technique for the case that input pulse has large pulse width. Next, in the Section III, we analyze the coding performances of these two kinds of en/decoders and the hybrid use of them. In the Section IV, we introduce the experimental demonstration of the performances of the 0/π-SSFBG and ± π/2-SSFBG en/decoders and the hybrid use of both en/decoders in the on-off keying (OOK) and differential phase-shift keying (DPSK) OCDMA systems.

#143119 - $15.00 USD Received 23 Feb 2011; revised 27 May 2011; accepted 1 Jun 2011; published 9 Jun 2011

2. Security performance

2.1 Security improvement

We develop a set of different gratings to test the performances, as tabulated in the Table 1. Four pairs of 0/π-SSFBG and ± π/2-SSFBG en/decoders with two same code sequences have the chip length of 0.156 mm, corresponding to the chip duration of 1.56 ps, and other two pairs of en/decoders have the chip length of 0.5 mm. 31-chip gold codes are used as the code patterns.

Table 1. Different SSFBG En/Decoder Used in the Experiment

Grating	Type	Code Sequence	Chip Length (mm)
CG1:CG1*	0/π-SSFBG	Gold code 1	0.156
CG2:CG2*	0/π-SSFBG	Gold code 2	0.156
NG1:NG1*	± π/2-SSFBG	Gold code 1	0.156
NG2:NG2*	± π/2-SSFBG	Gold code 2	0.156
CG5:CG5*	0/π-SSFBG	Gold code 2	0.5
NG5:NG5*	± π/2-SSFBG	Gold code 2	0.5

* indicates the decoder

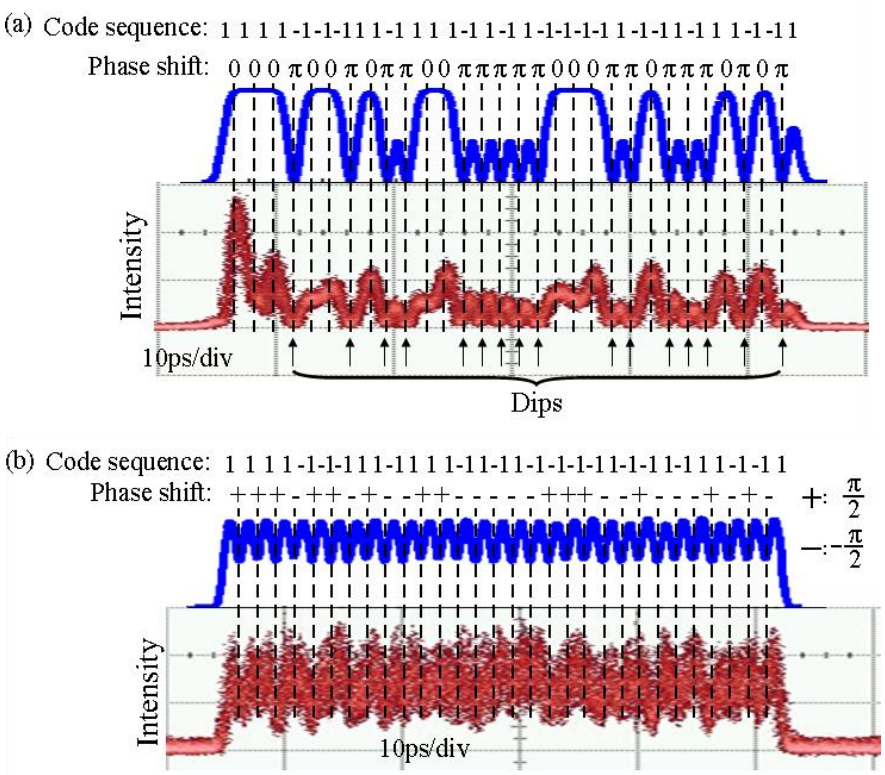

Fig. 1. Encoded waveforms of 0/π-SSFBG and ± π/2-SSFBG encoders with different chip durations (a) CG1 and (b) NG1.

#143119 - $15.00 USD Received 23 Feb 2011; revised 27 May 2011; accepted 1 Jun 2011; published 9 Jun 2011

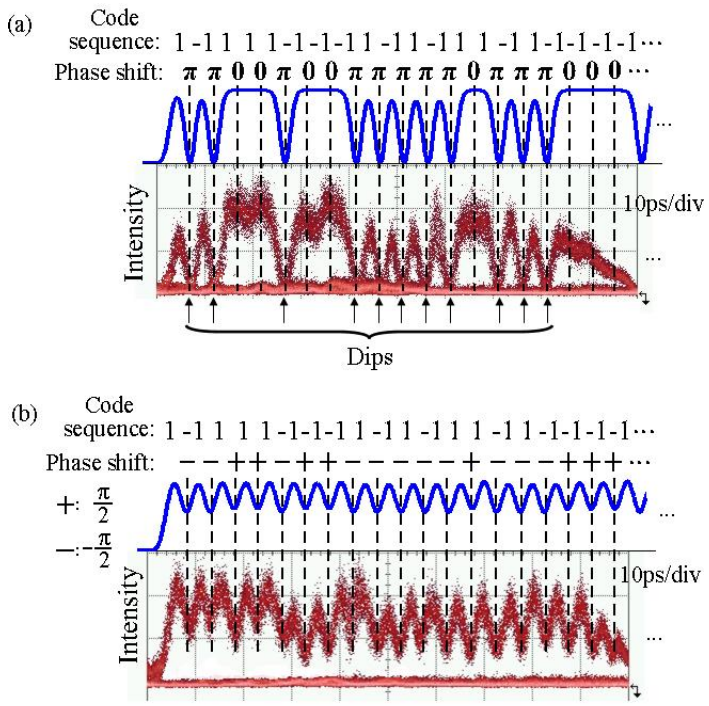

Fig. 2. Encoded waveforms of 0/π-SSFBG and ± π/2-SSFBG encoders with different chip durations (a) CG5 and (b) NG5.

In the experiment, we generate the Gaussian shaped optical pulse with the pulse width of 1 ps (FWHM) and launch into the 0/π-SSFBG and ± π/2-SSFBG encoders (CG1 and NG1) to investigate the security of the encoded waveforms, as shown in the Fig. 1. The calculated results are also shown above the experimental results. The measured waveforms fit the calculated results well. Dips can be easily found in the waveform encoded by the 0/π-SSFBG encoder. The existence of the dips hints the π phase shifts in the code pattern and results in the vulnerable regularity, based on which the thirty phase shifts can be determined. Then, the whole code sequence can be extracted accordingly. In the Fig. 1(b), 31 chips exhibit same peaks and valleys and no regularity can be found in the encoded waveform, which improves the security of the encoding.

To investigate the encoded waveform for different codes and chip length, we inject a 2.8 ps (FWHM) Gaussian shaped pulse into CG5 and NG5 encoders, whose chip duration are 5 ps. Due to the limited scope (100 ps) of the sampling oscilloscope, we use the Mach-Zehnder intensity modulation (IM) to truncate the encoded waveforms to the first 20 chips, which are shown together with the calculated results in the Fig. 2(a) and 2(b). The decline at the end of the encoded waveforms is resulted from the truncation. The fluctuation in the encoded waveform of the ± π/2-SSFBG encoder is resulted from the error in the grating fabrication. Eavesdroppers can easily extract the code sequence from the encoded waveform of the 0/π-SSFBG encoder. However, it is hard for eavesdroppers to figure out the code sequence used in the ± π/2-SSFBG encoder.

The ± π/2-SSFBG encoder conceals the code sequences well in the uniform encoded waveform, significantly improving the security of the coding. It is worth noting that [14] presented quaternary phase coding gratings, which also included ± π/2 phase shifts. But the ± π/2 phase shifts in these gratings are part of the quaternary code and contain the code information, so the code pattern could be partially extracted, while the phase shifts in the

#143119 - $15.00 USD Received 23 Feb 2011; revised 27 May 2011; accepted 1 Jun 2011; published 9 Jun 2011

proposed ± π/2-SSFBG are independent of code and undistinguishable in the encoded waveform. In this paper, we only focus on the binary phase coding gratings.

2.2 Influence of input pulse

The vulnerable regularity in the encoded waveform of the 0/π-SSFBG encoder is related to the structure of the encoder, which is independent of the input pulse. However, it has been found that the input pulse has the influence over the encoded waveform of the ± π/2-SSFBG encoder [12]. The intensity of the pulse reflected from the subgrating is variable with the change of the input pulse width, since neighboring reflected pulses have some influence over the middle one. When the chip duration of the ± π/2-SSFBG is fixed, with the increase of the pulse width, the reflected pulse within two different phase shifts grows, while that within same phase shifts decays relatively.

Apparently, an eavesdropper can utilize the relationship between the disparity of reflected pulse and phase shift to find out the code pattern. We summarize the code extraction technique for the ± π/2-SSFBG encoder as follows.

1) Partition the encoded waveform into N sections, where N is the number of chips.

2) Determine the intensity levels for the raised and decayed pulses, I_R and I_D and set the extraction level, $I_E = (I_R + I_D)/2$.

3) Assume the first phase shift to be + π/2 or –π/2. The assumption will result in two non-equivalent code sequences extracted from the waveform.

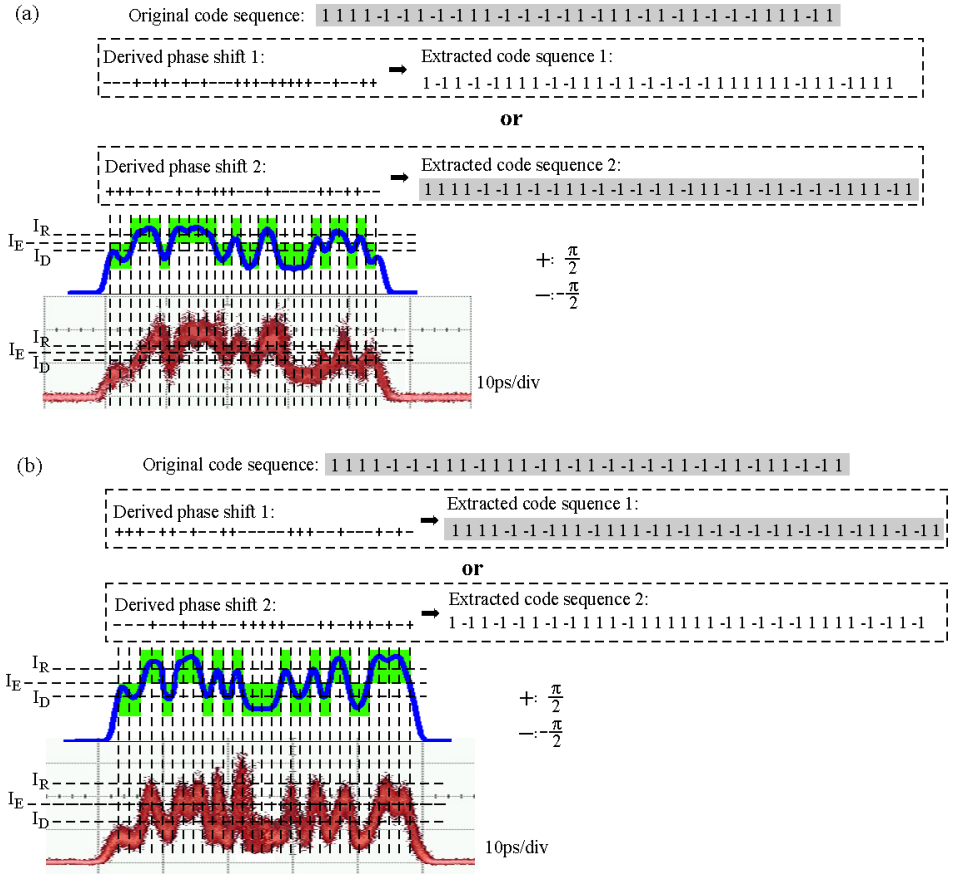

Fig. 3. Demonstration of code extraction technique for the ± π/2-SSFBG encoders (a) NG1 and (b) NG2.

#143119 - $15.00 USD Received 23 Feb 2011; revised 27 May 2011; accepted 1 Jun 2011; published 9 Jun 2011

4) Derive the next phase shift. If the intensity of next reflected pulse is above the extraction level, the next phase shift is different from the previous one, and vice versa.

5) Repeat Step 4 until all phase shifts are found.

6) Set the code in the first chip as mark '1'.

7) Find out the code in the next chip. If the phase shift is + $\pi/2$, the next code is same as the previous one, and it is different when the phase shift is $-\pi/2$

8) Repeat Step 7 until the whole code sequence is found.

9) Two code sequences are obtained due to the assumption of the first phase shift. To ascertain the real code sequence, decode the encoded signal with one code sequence. If the trial code sequence is the correct one, an autocorrelation peak can be observed.

To demonstrate the code extraction technique for the ± $\pi/2$-SSFBG encoder, we launch a 1.7 ps (FWHM) Gaussian shaped optical pulse into the encoders (NG1 and NG2). In the encoded waveforms, as illustrated in Fig. 3, the reflected pulses have different intensities. In the code extraction process, the chip positions are firstly located and the intensity levels of the raised and decayed pulses are estimated, from which the extraction level I_E is calculated. Then two groups of phase shift can be obtained. According to the two groups of phase shift, two non-equivalent code sequences are found. The two code sequences can generate the same waveform and the real one is not distinguishable from the encoded waveform. To confirm the real code sequence, the eavesdropper has to fabricate an SSFBG decoder to perform autocorrelation. Only the decoder with the real code sequence can generate the autocorrelation.

By comparison, the 0/π-SSFBG encoder cannot provide security in substance, since the eavesdropper can always find the dips in the encoded waveform and extract the code sequence, while the ± $\pi/2$-SSFBG encoder can conceal the code pattern well in the encoded waveform and guarantee the security by nature. In the case of the ± $\pi/2$-SSFBG encoder, theoretically, the discrepancy between the reflected pulses is reduced with the decrease of the input pulse width [12]. For example, when the input pulse width is half of the grating chip duration, the discrepancy is smaller than 0.1 dB. In the practical situation, the discrepancy can be neglected with the existence of fabrication error, system noise and transmission distortion, and the security can be ensured. In the case of Fig. 1(b), the input pulse width is 1 ps and the ± $\pi/2$-SSFBG has the chip duration of 1.56 ps. According to the theoretical calculation, the discrepancy is 0.35 dB. However, it is difficult to distinguish the raised and decayed pulses and tell the discrepancy. The extraction method is infeasible in the practical system when short input pulse is used and therefore the security can be guaranteed.

3. Coding performance

Besides the security performance, we also investigate the coding performance of both 0/π-SSFBG and ± $\pi/2$-SSFBG en/decoders by evaluating the ratio of autocorrelation intensity peak over the maximum wing level (P/W) and to the maximum cross-correlation level (P/C). In our calculation, the SSFBG en/decoder has the chip duration of 1.56 ps and the input pulse has the pulse width of 1 ps. Subsets of 31-chip, 63-chip and 127-chip Gold codes are used.

Table 2. Average Values of Auto- and Crosscorrelation for Different En/decoder and Chip Length

En/decoder	31-chip		63-chip		127-chip	
	P/W	P/C	P/W	P/C	P/W	P/C
0/π-SSFBG	13.02	8.17	16.63	11.81	32.25	29.10
± $\pi/2$-SSFBG	13.05	8.34	16.58	12.03	32.46	29.36
Hybrid use		10.79		20.42		32.27

#143119 - $15.00 USD Received 23 Feb 2011; revised 27 May 2011; accepted 1 Jun 2011; published 9 Jun 2011

Figure 4 illustrates the superimposed normal density of P/W for three different code lengths and the average values are listed in the Table 2. The ± π/2-SSFBG en/decoder has the similar autocorrelation performance as the 0/π-SSFBG en/decoder. With the increase of the code length, the autocorrelation performance of both en/decoders improves and the code capacity expands. Compared to the 31-chip and 63-chip cases, the en/decoders using 127-chip Gold code has much better performance.

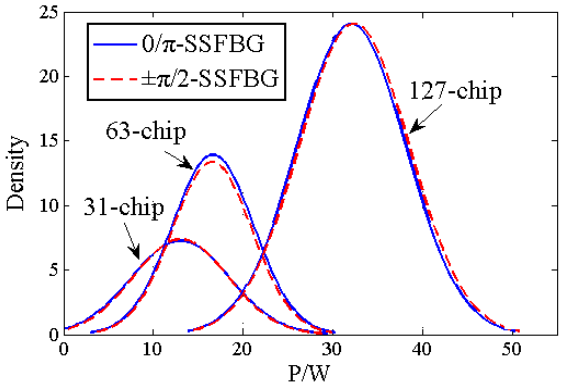

Fig. 4. Autocorrelation of the 0/π-SSFBG and ± π/2-SSFBG en/decoders with 31-chip, 63-chip and 127-chip Gold code.

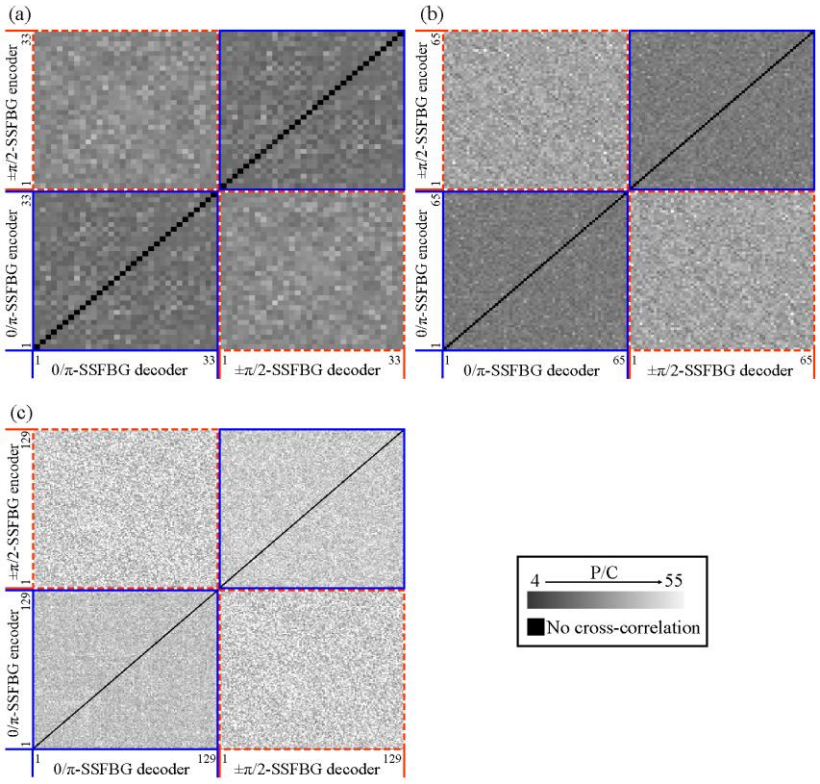

Fig. 5. Cross-correlation of the 0/π-SSFBG and ± π/2-SSFBG en/decoders and the hybrid use with (a) 31-chip, (b) 63-chip and (c) 127-chip Gold code.

#143119 - $15.00 USD Received 23 Feb 2011; revised 27 May 2011; accepted 1 Jun 2011; published 9 Jun 2011

The cross-correlation performance is depicted in Fig. 5 using the gray scale format, where brightness states the P/C value. In the bottom-left and top-right box, the cross-correlation performances of 0/π-SSFBG and ± π/2-SSFBG en/decoders are illustrated. According to the brightness, the ± π/2-SSFBG en/decoder presents the same cross-correlation performance as the 0/π-SSFBG en/decoder. The increased brightness and density with the different code length indicate the better performance and the larger code capacity.

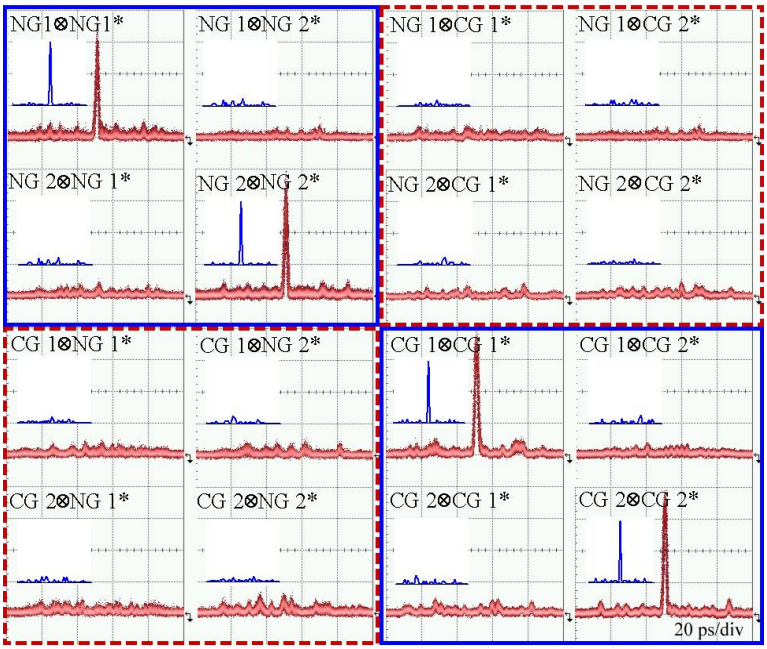

Fig. 6. Measured and calculated correlation of 0/π-SSFBG and ± π/2-SSFBG en/decoders.

Furthermore, we analyze the hybrid use of both en/decoders, i.e. 0/π-SSFBG encoder to ± π/2-SSFBG decoder and ± π/2-SSFBG encoder to 0/π-SSFBG decoder, whose cross-correlation performance is exhibited within the top-left and bottom-right box in Fig. 5. The average P/C values are tabulated in the Table 2. In the hybrid use, the sidelobes of the cross-correlation is low, which results in high P/C values. Due to the good cross-correlation performance of hybrid use, it guarantees that ± π/2-SSFBG en/decoder can be used together with 0/π-SSFBG en/decoder in the same system.

We measure the coding performance of the fabricated en/decoders. In the experiment, a 1 ps Gaussian shaped optical pulse was launched into the encoder and the decoder followed the encoder directly. Both measured and calculated decoded waveforms are shown in Fig. 6. The decoded waveforms of 0/π-SSFBG and ± π/2-SSFBG en/decoders are in the top-left and bottom-right box and the waveforms of the hybrid use is in the bottom-left and top-right box. An autocorrelation high peak is generated, if the decoder matches the encoder. Otherwise, a cross-correlation low power signal is produced. The hybrid use of the 0/π-SSFBG and ± π/2-SSFBG en/decoders also leads to the low power level cross-correlation. The P/W and P/C are all larger than 7. The good correlation guarantees the coding performance of both en/decoders and promises the hybrid use of the 0/π-SSFBG and ± π/2-SSFBG en/decoders.

The code recognition in SSFBG is aperiodic correlation, but the code sets used in the OCDMA system are designed for good periodic correlation properties. The number of codes with good aperiodic correlation is limited [8]. The hybrid use of both kinds of en/decoders is capable of reusing the same codes. According to our calculation and experimental measurement, even though 0/π-SSFBG and ± π/2-SSFBG en/decoders use the same code, they still perform good cross-correlation. It allows the same code being used twice in the same

#143119 - $15.00 USD Received 23 Feb 2011; revised 27 May 2011; accepted 1 Jun 2011; published 9 Jun 2011

system. Therefore, the hybrid use makes it possible to enlarge the number of the available codes.

4. System performance

4.1 2-user 10Gbps/user OOK-OCDMA system

To investigate the performances of the 0/π-SSFBG and ± π/2-SSFBG en/decoders in the system, we placed the en/decoders in a 2-user OOK-OCDMA system. The experimental setup is shown in Fig. 7. The mode locked laser diode (MLLD) generated a Gaussian shaped pulse train with the pulse width of 2.3 ps (FWHM) at a repetition rate of 10 GHz, spectrally centered at 1563 nm. After a 2 km dispersion flattened fiber (DFF) and a 7.5 nm band-pass filter (BPF), the pulse width was compressed to 1 ps. The pulse train was modulated with the 2^{15}–1 pseudorandom bit sequence (PRBS) data by the IM. The modulated pulse train was split into two arms. Two 0/π-SSFBG encoders (CG1 and CG2) or two ± π/2-SSFBG encoders (NG1 and NG2) were applied for the encoding. A 20 m single mode fiber (SMF) was added for de-coherence and an attenuator was used to balance the power of the encoded signals in the both arms. Then the encoded signals were combined for decoding. In the decoding section, corresponding decoder was used.

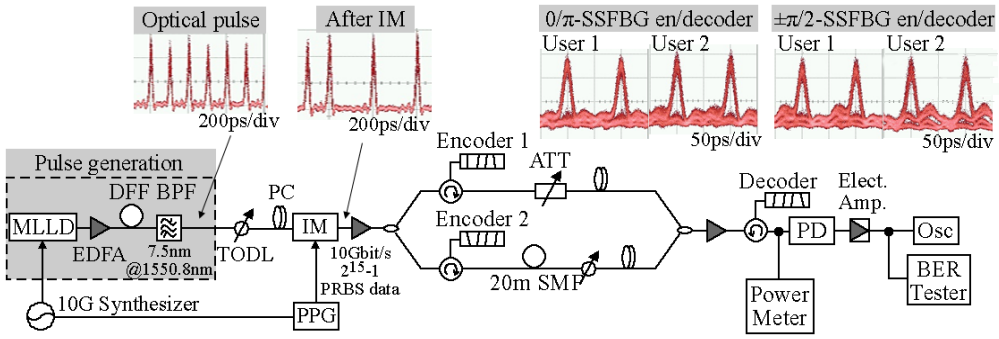

Fig. 7. Experimental setup of 2-user OOK-OCDMA system and measured waveforms and eye diagrams.

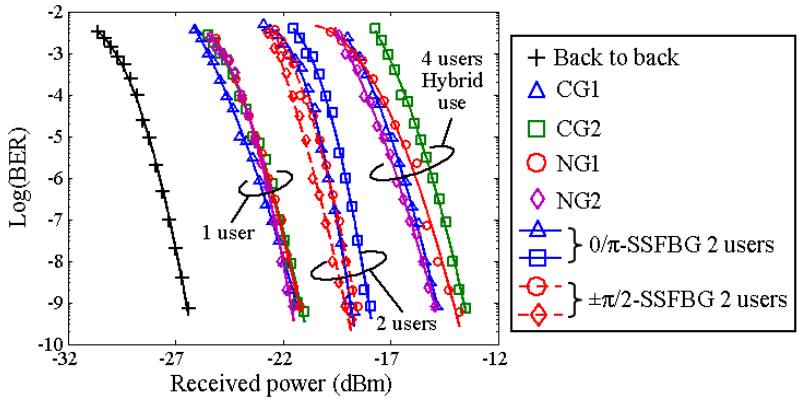

Fig. 8. BER performance of the 0/π-SSFBG and ± π/2-SSFBG en/decoders in the OOK-OCDMA system.

The bit-error-rate (BER) measurement against the received power is illustrated in Fig. 8. Both 0/π-SSFBG and ± π/2-SSFBG en/decoders achieve the error-free (BER<10-9). Relative to the single-user OOK-OCDMA system, the 2-user system has about 3 dB power penalty,

#143119 - $15.00 USD Received 23 Feb 2011; revised 27 May 2011; accepted 1 Jun 2011; published 9 Jun 2011

which is resulted from the multiple access interference (MAI) [15]. Compared to the 0/π-SSFBG en/decoder, ± π/2-SSFBG en/decoder has equally good performance in the system.

4.2 4-user 10Gbps/user OOK-OCDMA system with hybrid use of 0/π- and ± π/2-SSFBG en/decoders

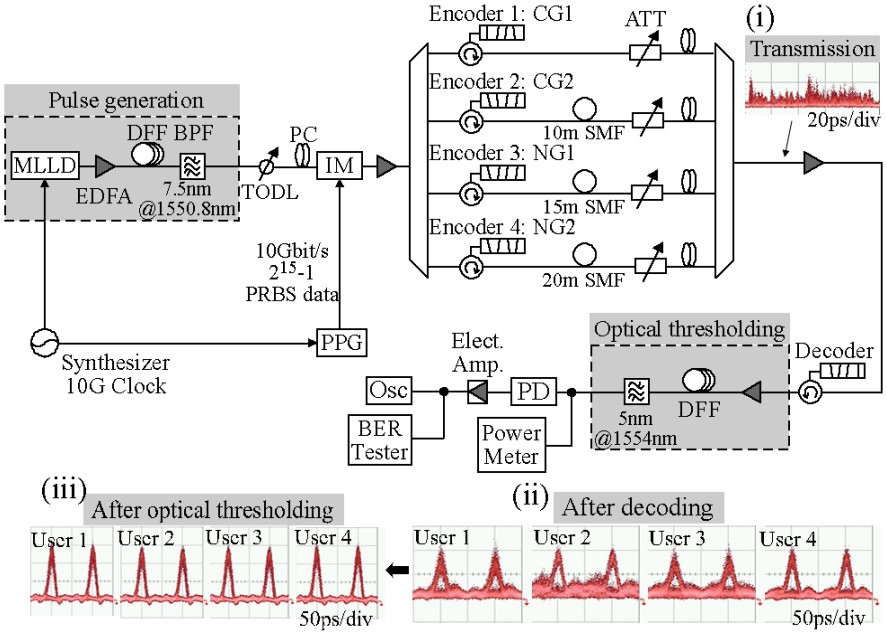

Fig. 9. Experimental setup of 4-user OOK-OCDMA system with hybrid use of en/decoders and measured waveforms and eye diagrams.

To investigate the hybrid use of the 0/π-SSFBG and ± π/2-SSFBG en/decoders in the same system, we modified the experimental setup according to Fig. 9. Two 0/π-SSFBG encoders and two ± π/2-SSFBG encoders were simultaneously utilized for the encoding. The encoded signals were multiplexed to generate the 4-user OOK-OCDMA signals, which exhibited as noise-like waveforms, as shown in the inset Fig. 9(i). In the receiving side, four decoders were used one by one to decode the multiplexed signal. When the decoder matched the encoder, the target signals were recovered into the high intensity peaks and the signals from other users resulted in the MAI noise, as illustrated in the inset Fig. 9(ii). To suppress the interference from other users, the super-continuum (SC) based optical thresholding was adopted, which consisted of an amplifier, a 2000 m DFF and a 5 nm BPF with the center wavelength of 1554 nm [16]. The MAI was efficiently removed by the optical thresholding (see inset Fig. 9(iii)). Clear eye diagrams for four users could be observed. The BER of four users is also depicted in Fig. 8. Compared to the single-user system, the four-user system causes about 7 dB power penalty at the BER of 10-9. The 10-9 BER of four users confirms the feasibility of the hybrid use of the 0/π-SSFBG and ± π/2-SSFBG en/decoders.

4.3 4-user 10Gbps/user DPSK-OCDMA system with hybrid use of 0/π- and ± π/2-SSFBG en/decoders

We also study the performance of the en/decoders in the 4-user 10Gbps/user DPSK-OCDMA system with the optical time gating detection, whose experimental setup is shown in Fig. 10. The pulse train from the SC source was divided into two branches. One was filtered at 1550.8 nm and modulated with the 2^{15}–1 pseudorandom bit sequence (PRBS) data by the phase modulator (PM). The modulated pulse train was divided into four arms for encoding and

#143119 - $15.00 USD Received 23 Feb 2011; revised 27 May 2011; accepted 1 Jun 2011; published 9 Jun 2011

combined to generate the 4-user DPSK-OCDMA signals. At the receiver, the multiplexed signals were decoded by the corresponding decoders, followed by the optical time gating detection. Optical time gating is capable to efficiently remove the MAI noise in an OCDMA system [17–19]. In the optical time gating section, the decoded signals were combined by a 3 dB coupler with the pump pulses, which were from another branch of the SC source and filtered at 1563 nm. The combined signals were launched into the highly nonlinear fiber (HNLF) for four-wave mixing (FWM). A 5 nm filter centered at 1574 nm passed the target signals. After the time gating, the MAI was mitigated and the target signals were detected by the balanced photodetector.

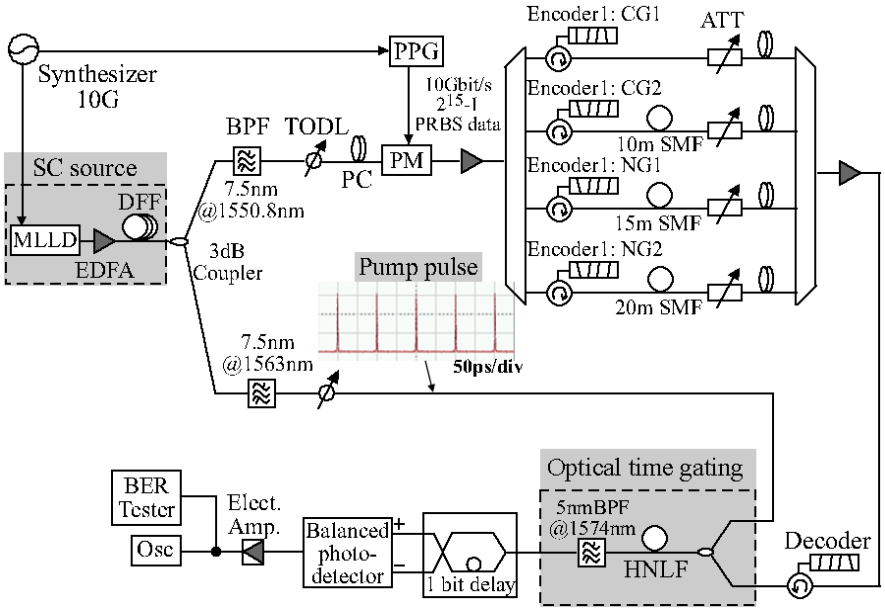

Fig. 10. Experimental setup of 4-user DPSK-OCDMA system with hybrid use of en/decoders and measured waveforms and eye diagrams.

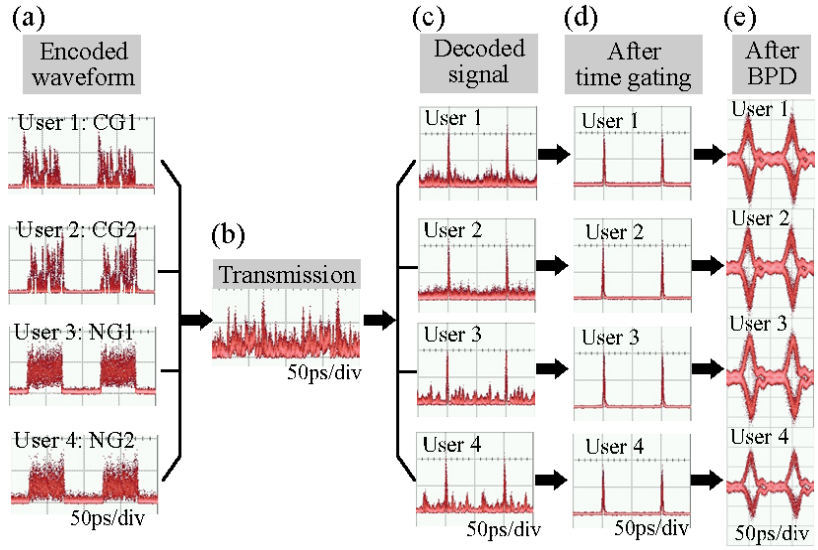

Fig. 11. Measured waveforms and eye diagrams in the 4-user DPSK-OCDMA system.

#143119 - $15.00 USD Received 23 Feb 2011; revised 27 May 2011; accepted 1 Jun 2011; published 9 Jun 2011

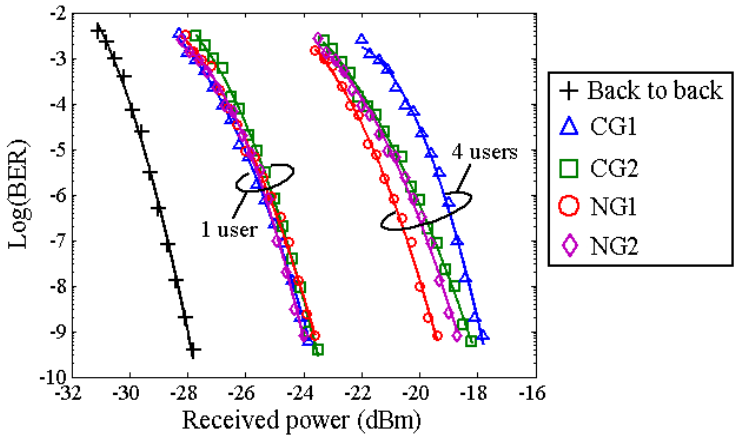

Fig. 12. BER performance of the 0/π-SSFBG and ± π/2-SSFBG en/decoders in the DPSK-OCDMA system.

The measured waveforms at different points of the experiment are illustrated in the Fig. 11. The encoded waveforms of the 0/π-SSFBG encoders are distinguishable, while the waveforms encoded by the ± π/2-SSFBG encoders have the uniform shapes, as shown in Fig. 11(a). Comparing the waveforms in Fig. 11(c) with those in Fig. 11(d), we can see that the MAI can be well suppressed by means of the time gating. Clear open eye diagrams can be obtained after the balanced detection, shown in Fig. 11(e). Figure 12 shows the BER performance for the hybrid use of the 0/π-SSFBG and ± π/2-SSFBG en/decoders in the DPSK-OCDMA system. Error-free has been achieved for all the four users and the 4-user system has a 6 dB power penalty compared to the single-user system. The ± π/2-SSFBG en/decoder performs as well as the 0/π-SSFBG en/decoder. The error-free achieved in the experiment promises that the hybrid use of both en/decoders is also feasible in the phase modulated system.

5. Conclusion

We have demonstrated the security performance of both 0/π-SSFBG and ± π/2-SSFBG en/decoders. The existence of dips in the encoded waveform of 0/π-SSFBG encoder makes it easy for eavesdroppers to extract the code sequence, while the uniform waveform encoded by the ± π/2-SSFBG encoder significantly improves the security. We also have analyzed the influence of the input pulse over the encoded waveform of the ± π/2-SSFBG encoder and discussed the code extraction technique when the input pulse has large pulse width. We emphasize that the short input pulse is a key point to guarantee the security.

In the aspect of the coding performance, we have theoretically calculated the correlation performance of both en/decoders with 31-chip, 63-chip and 127-chip Gold codes. The ± π/2-SSFBG en/decoder exhibits as good performance as the 0/π-SSFBG en/decoder does. Importantly, we have proposed the hybrid use of both en/decoders and investigated its coding performance. Furthermore, we have demonstrated the coding performance of four fabricated 31-chip 640 Gchip/s 0/π-SSFBG and ± π/2-SSFBG en/decoders. The good correlation performance of the hybrid use ensures the reutilization of the available codes in the same code space.

In addition, we have carried out proof of principle experiments to investigate the performance of the 0/π-SSFBG and ± π/2-SSFBG en/decoders in the multi-user OOK- and DPSK-OCDMA systems. The achieved error-free transmissions in different systems confirm the acceptable performances of the ± π/2-SSFBG en/decoder and the hybrid use of both en/decoders.

#143119 - $15.00 USD Received 23 Feb 2011; revised 27 May 2011; accepted 1 Jun 2011; published 9 Jun 2011

Acknowledgments

This work was supported by the Royal Society International Joint Projects. The authors would like to thank Mr. H. Sumimoto of NICT for his technical support. Zhensen Gao also acknowledges the international travel grant by the Royal Academy of Engineering.

#143119 - $15.00 USD Received 23 Feb 2011; revised 27 May 2011; accepted 1 Jun 2011; published 9 Jun 2011